European **J**ournal of **Chem**istry

Check for updates

Crystal structure, Hirshfeld surface, and DFT studies of 4-((pyrrolidin-1-ylsulfonyl)methyl)aniline

Soundararajan Krishnan [iD] [1], Thanigaimani Kaliyaperumal [iD] [2], Ramalingam Marimuthu [iD] [3] and Sethuraman Velusamy [iD] [1,*]

[1] *Department of Chemistry, Periyar Maniammai Institute of Science and Technology, Vallam - 613 403, Thanjavur, Tamil Nadu, India*
soundardk87@gmail.com (K.S.), xrdsethu@gmail.com (V.S.)
[2] *Department of Chemistry, Government Arts College, Tiruchirappalli - 620 022, Tamil Nadu, India*
thanigaimani81@gmail.com (K.T.)
[3] *Department of Chemistry, Bon Secours College for Women, Thanjavur - 613 006, Tamil Nadu, India*
km_ramalingam@yahoo.co.in (M.R.)

* Corresponding author at: Department of Chemistry, Periyar Maniammai Institute of Science and Technology, Vallam - 613 403, Thanjavur, Tamil Nadu, India.
 e-mail: xrdsethu@gmail.com (S. Velusamy).

RESEARCH ARTICLE

ABSTRACT

The crystal structure investigation of the title compound 4-((pyrrolidin-1-ylsulfonyl) methyl)aniline (PSMA) $C_{11}H_{16}N_2O_2S$ shows that the molecule is essentially coplanar with a dihedral angle of 26.70(14)° between the pyrrolidine and the benzene rings. A pair of strong N-H···O hydrogen bonds produces continuous two-dimensional sheets with $R_2^2(18)$ ring motifs. The crystal structure also features a weak C-H···π interaction resulting in a three-dimensional network. Density functional theory (DFT) calculations reveal that the experimental and calculated geometric parameters of the molecule are nearly the same. Hirshfeld surface analysis has been carried out to study the various intermolecular interactions responsible for the crystal packing. Theoretical calculations indicate an excellent correlation between the experimental and the simulated UV spectra.

Cite this: *Eur. J. Chem.* **2021**, *12(4)*, 419-431 **Journal website**: www.eurjchem.com

1. Introduction

Aromatic amines and their derivatives are of great importance in various fields such as biology, agriculture, pharmaceutics, and industry. Acetanilide and phenacetin were used as analgesic and cardiac drugs along with caffeine [1]. After the discovery of the first 'miracle drug' prontosil in 1932 [2], numerous sulfa drugs emerged during the Second World War. Sulfa drugs are sulfonamides that contain the $-SO_2NH_2$ and/or $-SO_2NH-$ group(s) that inhibit the synthesis of folic acid in microorganisms [3]. A wide range of aryl- and heteroaryl sulfonamides having different biological activities have been synthesized [4-9]. They have a spectrum of pharmacological properties, such as antitumor [10], antibacterial [11], anti-carbonic anhydrase [12,13], diuretic [14,15], hypoglycemic [16], protease inhibitory activities [17-19] and antithyroid activity [20]. They are also used for the treatment of tonsillitis, septicemia, meningococcal meningitis, bacillary dysentery and urinary tract infections [21].

The substituents and their position in the benzene ring of sulfonamides determine the antimicrobial activity. Sulfon-amides are bacteriostatic in nature. Microorganisms require *p*-amino benzoic acid (PABA) for the synthesis of folic acid involved in the synthesis of DNA and RNA. Sulfonamides inhibit PABA due to their structural resemblance which causes folic acid deficiency, resulting in inhibition of bacterial growth and cell division [21].

Most of the sulfa drugs are secondary sulfonamides, and some examples of the drugs having *p-aminobenzene derivatives* are almotriptan, sulfapyridine, sulfamethoxazole, and sulfa-diazine.

4-(Pyrrolidin-1-ylsulfonyl)methyl)aniline is the starting material of almotriptan, the structures of both being shown in Figure 1a and b, which is a selective serotonin 5-HT1B/1D receptor agonist and is a second generation triptan (Trypt-amine-based drug) used in acute treatment of migraine attacks [22]. The crystallographic, computational, and Hirshfeld surface analysis of PSMA have been undertaken in the present work.

Table 1. Crystal data and structure refinement for PSMA.

Empirical formula	$C_{11}H_{16}N_2O_2S$
Formula weight	240.32
Temperature (K)	293(2)
Crystal system	Monoclinic
Space group	$P2_1/n$
a, (Å)	13.736(5)
b, (Å)	5.807(5)
c, (Å)	16.079(5)
α (°)	90.000(5)
β (°)	112.351(5)
γ (°)	90.000(5)
Volume (Å³)	1186.2(12)
Z	4
ρ_{calc} (g/cm³)	1.346
μ (mm⁻¹)	0.261
F(000)	512.0
Crystal size (mm³)	0.3 × 0.2 × 0.2
Radiation	MoKα (λ = 0.71073)
2Θ range for data collection (°)	3.34 to 49.96
Index ranges	-15 ≤ h ≤ 16, -6 ≤ k ≤ 6, -19 ≤ l ≤ 19
Reflections collected	10904
Independent reflections	2081 [R_{int} = 0.0285, R_{sigma} = 0.0212]
Data/restraints/parameters	2081/0/154
Goodness-of-fit on F²	1.143
Final R indexes [I≥2σ (I)]	R_1 = 0.0347, wR_2 = 0.1024
Final R indexes [all data]	R_1 = 0.0443, wR_2 = 0.1235
Largest diff. peak/hole (e.Å⁻³)	0.31/-0.19
CCDC Number	2100572

Table 2. Hydrogen bond for PSMA.

D-H···A	D-H (Å)	H···A (Å)	D···A (Å)	∠ D-H···A (°)	Symmetry code
N1-H1A···O1	0.84(3)	2.48(3)	3.243(4)	151(3)	3/2-*x*, -1/2+*y*, 1/2-*z*
N1-H1B···O2	0.86(4)	2.47(3)	3.241(4)	151(3)	3/2-*x*, 1/2+*y*, 1/2-*z*

Figure 1. Structures of (a) PSMA and (b) almotriptan.

2. Experimental

2.1. Crystal preparation

The crystal was prepared by mixing 4-((pyrrolidin-1-ylsulfonyl)methyl)aniline compound (TCI Chemicals India Pvt. Ltd.) with aqueous methanol and heating the mixture for a few minutes. The solution was warmed at 50 °C for half an hour in a water bath. The resultant solution was allowed to cool by slow evaporation. After two days, blocks of yellow colored crystals were separated [23].

2.2. Single-crystal x-ray structure determination

A Bruker Kappa APEX-II CCD diffractometer having monochromatic MoKα radiation (λ = 0.71073 Å) was used for single crystal X-ray diffraction data collection. Bruker SAINT [24] was then involved in the integration followed by and corrections for Lorentz and polarization effects. For absorption correction, the multi-scan method using SADABS [24] was utilized. SHELXS97 [25] software had been used to get the structure solution by direct method and the refinement had been carried out by full matrix least squares on F^2 using SHELXL-2014/7 [26]. After the non-H atoms were refined with anisotropic factors, the hydrogen atoms were positioned geometrically and refined isotropically as riding on their carrier atoms. Relevant crystal data and details of the hydrogen bond framework have been collected in Tables 1 and 2.

2.3. DFT studies

For all computations, the B3LYP of density functional theory was followed [27] through the Gaussian 03W/09W [28,29] suite of programs. This level of computation, despite its inability to reproduce dispersive forces accurately [30] was chosen because DFT is computationally non-expensive and gives reliable results. To account suitably for orbital contraction in the molecular environment, diffuse nature of non-bonding electrons, and shifting the centre of orbitals in small rings, the well-known 6-311++G(d,p) basis set, which is more adaptable in the valence region if hydrogen bond interaction is present, had been chosen. The initial geometrical structure constructed from the XRD coordinates was optimized by invoking gradient geometry optimization with complete relaxation. The optimized geometry at the stationary point was characterized by inspecting the absence of imaginary frequencies. In the gas phase as well as in the appropriate solvent (PCM model), vertical electronic excitation calculations have been done with time-dependent DFT.

2.4. Hirshfeld surface analysis

2.4.1. Hirshfeld surface

Hirshfeld's quantitative molecular charge distribution in terms of atomic fragments [31,32] led to propose a new scheme for partitioning of crystalline electron densities.
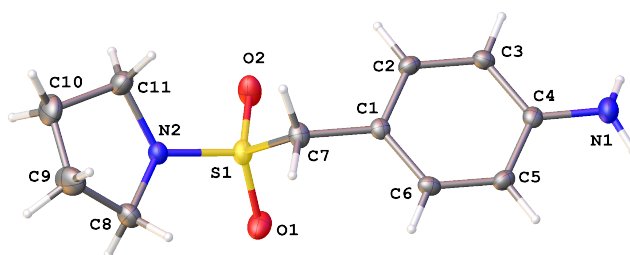
Figure 2. ORTEP view of the PSMA molecule.
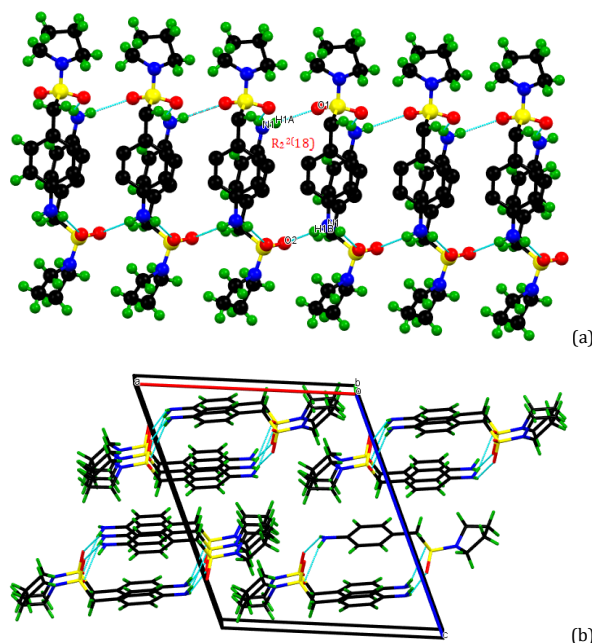
Figure 3. (a) H-bonded ring motif present in PSMA and (b) packing diagram of PSMA with its 3-dimensional hydrogen bond network.

As Hirshfeld's density weight function for an atom in a molecule, the weight function $w_A(r)$ for a molecule (promolecule) in a crystal is defined as [33-35].

$$w_A(r) = \frac{\sum_{i \in molecule\ A} \rho_i^{at}(r)}{\sum_{i \in crystal} \rho_i^{at}(r)} = \rho_{Promolecule}\ (r) / \rho_{Procrystal}\ (r) \qquad (1)$$

where $\rho_{promolecule}(r)$ sums over the electron density of atoms in the molecule of interest and $\rho_{procrystal}(r)$ is an analogous sum over the crystal (the procrystal). $w_A(r)$ is a continuous function with $0 < w_A(r) < 1$. An isosurface of $w_A(r)$, defined by $w_A(r) = 0.5$, HS - envelops the molecule, and defines the volume of space where the promolecule electron density exceeds that from all neighboring molecules. It guarantees the maximum proximity of neighboring molecular volumes, but the volumes never overlap because of the nature of the weight function. The shape of HS is a function of not only the intermolecular interactions of the crystal but also the interactions among the atoms of the promolecule.

2.4.2. Hirshfeld surface investigation

The CIF file generated after refinement of the structure in Shelx has been used in CrystalExplorer 17.5 to create the isosurface HS and fingerprint plots to perform an in-depth analysis of intermolecular contacts in addition to the various components of interaction energies, around the promolecule and the procrystal, encompassing the partitioning of crystalline electron densities.

3. Results and discussion

3.1. Crystal structure analysis

3.1.1. Molecular geometry

The asymmetric unit of the crystal of the title compound contains one PSMA molecule and the ORTEP view of the molecule is shown in Figure 2. The dihedral angle between the mean planes of the pyrrolidine and benzene ring systems is 26.70(14)°. The S1=O1 and S1=O2 bond lengths are identical with the values of 1.426(2)° and 1.427(2)°, respectively, which are in line with the known values. The S1-N2 and S1-C7 bond lengths are 1.607(3) and 1.779(3) Å, respectively, with an N2-S1-C7 bond angle of 106.49(10)°. The torsion angles of both the C-N bonds of the pyrrolidine ring to the S1-C7 bond are: C11-N2-S1-C7 = -171.70(17)° and C8-N2-S1-C7 = -72.21(19)°. A conformational analysis of the five-membered pyrrolidine ring gives a puckering amplitude ($\varphi 2$) parameter of 0.331(3)° and a ψ^2 parameter of 112.1(5)°. Consequently, this ring is in a half - chair conformation with a twist along C9-C10 bond. Generally, the bond lengths and angles are found to be normal [36].

3.1.2. Supramolecular features

In the crystal structure of the title compound, the molecules are linked by N-H···O hydrogen bonds and C-H···π interactions as shown in Figure 3a and b. Table 2 gives the hydrogen bond information.

Table 3. Comparison of the geometrical parameters calculated and experimental of PSMA.

Bond length (Å)	Calculated	Experimental	Bond Angle (°)	Calculated	Experimental
C1-C2	1.39911	1.385(3)	N11-C12-C13	103.006	104.3(2)
C2-C3	1.38807	1.370(4)	C12-C13-C14	103.371	106.393
C3-C4	1.40305	1.390(3)	C13-C14-C15	103.218	104.5(3)
C4-C5	1.40321	1.385(3)	C14-C15-N11	103.575	102.6(2)
C5-C6	1.38797	1.373(4)	C15-N11-C12	111.540	110.11(19)
C6-C1	1.39914	1.389(3)	O9-S8-O10	120.869	118.09(11)
C4-N16	1.39459	1.386(4)	C7-S8-N11	102.841	106.49(10)
C1-C7	1.49800	1.498(3)	**Dihedral Angle (°)**	**Calculated**	**Experimental**
C7-S8	1.84024	1.779(3)	C1-C2-C3-C4	-0.297	0.2(3)
S8-O9	1.46519	1.426(2)	C2-C3-C4-C5	0.252	-0.5(3)
S8-O10	1.46518	1.427(2)	C3-C4-C5-C6	-0.278	0.6(3)
S8-N11	1.67956	1.607(3)	C4-C5-C6-C1	0.350	-0.2(3)
N11-C12	1.48578	1.474(3)	C5-C6-C1-C2	-0.378	-0.2(3)
C12-C13	1.53385	1.489(5)	C6-C1-C2-C3	0.352	0.2(3)
C13-C14	1.53563	1.472(5)	C2-C3-C4-N16	177.445	-178.9(2)
C14-C15	1.53345	1.498(4)	C6-C5-C4-N16	-177.473	178.9(2)
C15-N11	1.48673	1.467(3)	C5-C6-C1-C7	-179.323	-179.07(19)
Bond Angle (°)	**Calculated**	**Experimental**	C6-C1-C7-S8	88.817	-105.94(19)
C1-C2-C3	121.222	121.4(2)	C2-C1-C7-S8	-90.097	75.3(2)
C2-C3-C4	120.561	121.3(2)	C1-C7-S8-O9	-65.674	67.35(18)
C3-C4-C5	118.393	117.4(2)	C1-C7-S8-O10	66.139	-62.02(18)
C4-C5-C6	120.581	121.4(2)	C1-C7-S8-N11	-179.683	-176.95(14)
C5-C6-C1	121.201	121.2(2)	C7-S8-N11-C12	104.554	-72.21(19)
C6-C1-C2	118.041	117.5(2)	C7-S8-N11-C15	-110.401	72.30(19)
C3-C4-N16	120.793	120.9(2)	O9-S8-N11-C12	-9.157	43.8(2)
C5-C4-N16	120.754	121.8(2)	O9-S8-N11-C15	135.888	-171.70(17)
C6-C1-C7	121.018	120.85(19)	O10-S8-N11-C12	-141.686	171.78(18)
C2-C1-C7	120.932	121.70(19)	O10-S8-N11-C15	3.358	-43.71(19)
C1-C7-S8	112.904	113.03(15)	S8-N11-C12-C13	162.094	150.8(2)
C7-S8-O9	107.680	108.27(11)	S8-N11-C15-C14	-137.214	-170.84(18)
C7-S8-O10	107.668	108.61(12)	N11-C12-C13-C14	-32.726	18.8(3)
O9-S8-N11	108.087	107.81(10)	C12-C13-C14-C15	39.509	-33.2(3)
O10-S8-N11	108.243	107.01(11)	C13-C14-C15-N11	-30.418	33.9(3)
S8-N11-C12	119.220	120.92(16)	C14-C15-N11-C12	10.267	-22.9(3)
S8-N11-C15	120.603	120.30(16)	C15-N11-C12-C13	14.110	3.0(3)
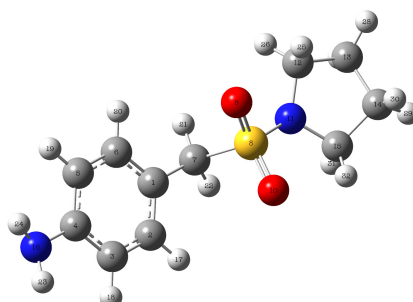
Figure 4. Numbering system adopted for computation in PSMA.

The two strong N-H···O hydrogen bonds are formed by the interaction of the amino nitrogen atom (N1) with the sulfonamide oxygen atoms O1 and O2 via a pair of N1-H1A···O1 and N1-H1B···O2 hydrogen bonds forming a ring motif of $R_2^2(18)$. The adjacent ring motifs are connected into sheets in the *bc*-plane. These adjacent sheets are further interconnected via weak C7-H7···π aryl interactions involving the centroid of the benzene ring with a distance of 3.587 Å between C···π which is less than the typical ~4.5 Å distance of hydrophobic contacts. All these interactions led to a three-dimensional network as shown in Figure 3.

An analysis of CSD reveals that there are five structures related to PSMA, four of them being directly related to Almotriptan, one being the structure of pure almotriptan [37] and the other three being the acid salts of almotriptan with malic acid [37], oxalic acid and terephthalic acid [38]. In all the three acid salts of almotriptan, protonation occurs only in the side chain amino group out of the three Nitrogen atoms available. It is of interest to know which nitrogen atom undergoes protonation in the absence of an amino side chain if acid salts are prepared for PSMA. The reasons for it can then be analyzed from the point of view of crystallography and

computation in future. If hydrated PSMA/salt crystals could be prepared, the role of water could be compared and explored.

3.2. Computational studies of PSMA

The PSMA molecule along with the atom numbering system adopted for computation is shown in the Figure 4. The different bond lengths, bond angles, and torsion angles theoretically calculated for the neutral PSMA are compared with the corresponding values experimentally observed by X-ray crystallography in the parent PSMA molecule. They are shown in the Table 3. In the case of PSMA also, the calculated and experimental bond lengths, bond angles, and torsion angles (θ/180-θ) are found to be in satisfactory agreement with one another.

3.3. Hirshfeld surface analysis

3.3.1. Hirshfeld surface (HS) mapping of PSMA

The HF isosurface defined by the isovalue $w_A(r) = 0.5$, mapped over the d_{norm} function of PSMA (-0.2061 to +1.3455
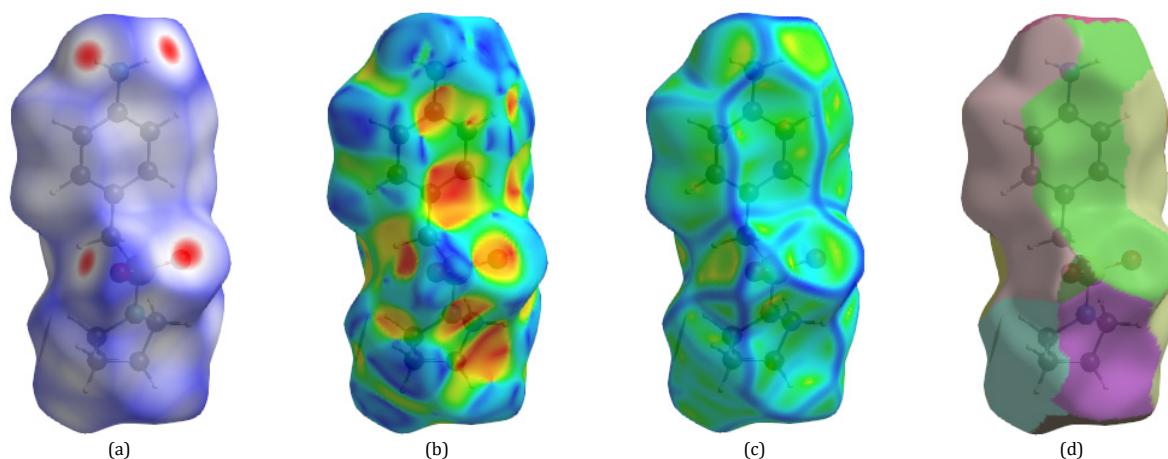
Figure 5. Hirshfeld surface mapped over (a) d_{norm}, (b) shape index, (c) curvedness, and (d) fragment patch.

Color														
Area (Å²)	15.5	28.5	47.4	18.4	8.1	30	7.7	19.7	32.4	1.2	0.7	29.3	2.5	31.2
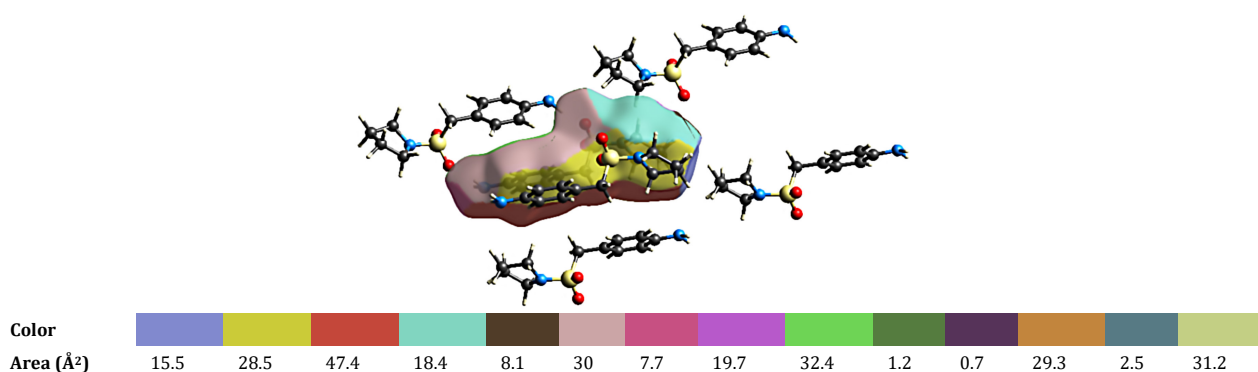
Figure 6. HSA-Coordination environment with their color patches.

arbitrary units; 0 < d_{norm} < 0 - indicative of r^{vdW} shorter/longer than the contact distance) from the CIF file is shown in Figure 5a holding a volume 290.61 Å³ and area 272.68 Å² along with shape index (-1.0 to 1.0 Å) (Figure 5b); curvedness (-4.0 to 0.4 Å) (Figure 5c) and fragment patch (0.0 to 13.9) (Figure 5d). d_{norm} is the sum of $d_i + d_e$ where d_i and d_e are the normalized extensions from a chosen point on the HS to the inside and outside atoms correspondingly.

The various color codes on the HS mapped onto the d_{norm} indicate the type of interatomic contacts/interactions, such as red, blue, and white colors corresponding to shorter, equal, and longer than the sum of the van der Waals radii of interacting/contacting atom pair [39].

The shape of the molecule exhibited by the HS, which is a function of the nearby crystalline environment of the pro-molecule, is generated with the shape index in the interval from -1.0 to +1.0 and is presented in Figure 1b [40]. The shape index is a qualitative measurement of the shape of the promolecule; it is sensitive to even small variations in the shape. The crest/convexity of the blue colored shape with negative shape index shows the H-bond interaction of donor type region (-NH₂), while its complementary region with a red trough acts as an acceptor (>SO₂). The aromatic C-H···π stacking in the crystal packing appears as red spot over benzene ring. The curvedness, *C* introduced [41] is a function of the root mean square curvature of the surface. Low curvedness above the benzene moiety has low coordination, while the area around -NH₂ and > SO₂ with moderate curvedness exhibits higher coordination. This is very clear in the differently colored fragment patches on the HS, mapped between the arbitrary units -4.0 and +4.0 shown in Figure 6. Of the 14 differently colored patches with a

specifically defined area, only 5 fragments around the HS are shown along with the color-coding scale.

Color patches on the Hirshfeld surface differently depend on their closeness to adjacent molecules. It provides a convenient way to identify the nearest neighbor coordination environment of a molecule (and hence its "coordination number"). The atoms within 3.8 Å from the HS of PSMA with their respective molecules, involving noncovalent interactions at various levels, displayed in different color codes as mentioned above are shown in Figure 6.

The strong hydrogen bond interactions with the sum of the van der Waals radii of participating atoms greater than the hydrogen bond lengths are marked as intense red colored circles on the HS, at > SO₂ and -NH₂ fragments of PSMA, where the former being the acceptors (lower red spots) and the latter being the donors (upper red spots) as shown in Figure 5a. This inference is evident from the hydrogen bond lengths of 2.337 and 2.340 Å corresponding to the hydrogen bond frameworks S-O2···H1B-N1 and S-O1···H1A-N1 values falling below the sum of O and H van der Waals radii of 2.72 Å [42]. The bond angles subtended by these two hydrogen bond frameworks are the same, namely 148.6° and hence the magnitude of the interaction would also be the same. Additionally, O2 involves the non-bonded interaction with H7-C7 fragment displaying the H-bond type interaction O2···H7B-C7 with H-bond geometrical parameters 2.606 Å and 166.7°. Despite the fact that geometrical factors favor more the O2···H7B-C7, the electro-negativity of N in S-O2···H1B-N1 overweighs the former. Figure 7 is giving different views of hydrogen bond interactions shows the pro-molecule's > SO₂ and -NH₂ are in close contact with the nearby PSMA molecules' -NH₂ and > SO₂ moieties.

(a)

(b)

(c)
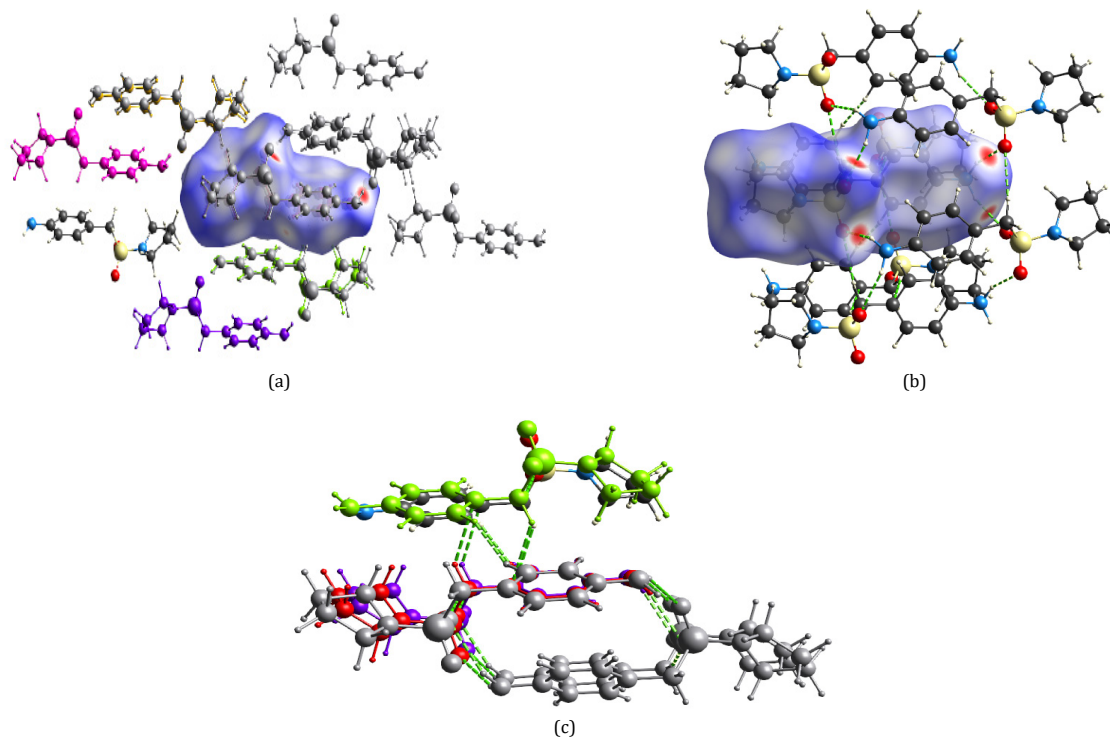
Figure 7. HSA-Hydrogen bonding interactions, (a) Display of all interacting molecules within 3.8 Å, (b) Display of strong H-bonded interactions, and (c) Display of hydrogen bonded pattern.

(a)

(b)
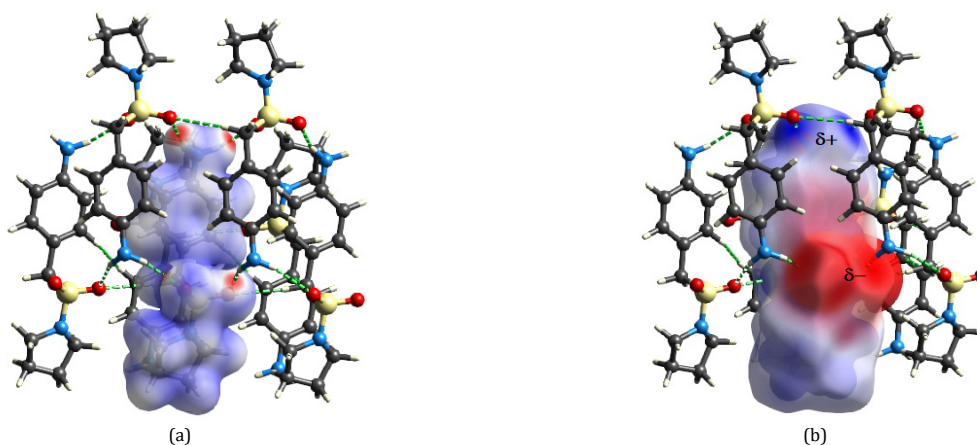
Figure 8. (a) HSA-Electron density map and (b) HSA-Electrostatic potential map.

Unlike > SO_2 fragment, -NH_2 does not have a fork-type hydrogen bond framework. As the C7-H7A···C1 interaction is weak, the region around that area is white colored in spite of the H7A...C1 distance of 2.759 Å / being less than the sum of van der Waals radii of 2.9 Å, to the extent of 0.149 Å. The very weak interactions with a contact distance greater than the sum of the van der Waals radii of participating atoms are shown as blue regions.

3.3.2. Electron density

The Tonto incorporated in CrystalExplorer 17.5 was invoked to compute the wavefunction at B3LYP/5-31G(d, p) and then to map the electron density of the promolecule onto the HS. Figure 8a shows the 3D electron density, which helps to identify the donor and acceptor region in red. Figure 8b displays the electrostatic potential surface constructed with the wave function generated through Tonto at B3LYP/6-31G(d,p)

over the pro-molecule, ensuring the intermolecular strong H-bond interactions with acceptor > SO_2 fragment (red color region) and donor -NH_2 unit (blue color region).

3.3.3. Electrostatic deformation density

The electrostatic deformation density map of Figure 9 shows the electron density about one molecule of PSMA. The deformation density represents a difference between the total electron density of a molecule and the electron density of "neutral spherical unperturbed atoms" superimposed on the same molecule [43,44]. The wave function calculated with Tonto ay B3LYP/6-31G(d,p) reveals the charge dearth region (in red) over -NH_2 unit, enabling N-H···O contacts in the crystal, while the charge excess (in blue) around >SO_2, makes O···H-N interaction. These interactions are shown in Figure 9b where the P molecule is surrounded by nearest six E1 to E6 molecules in the crystalline state.

Table 4. The breakup details of 2D fingerprint area of interaction into individual type (Percentage)-for close contacts between atoms inside and outside the HS.

HF in	HF out					
	C	**H**	**N**	**O**	**S**	**Total**
C	0.4	8.9	.	.	.	9.3
H	7.5	53.7	2.5	11.0	0.0	74.8
N	.	2.6	.	.	.	2.6
O	.	13.3	.	.	.	13.3
S	.	0.0	.	.	.	0.0
Total	7.9	78.5	2.5	11.0	0.0	100
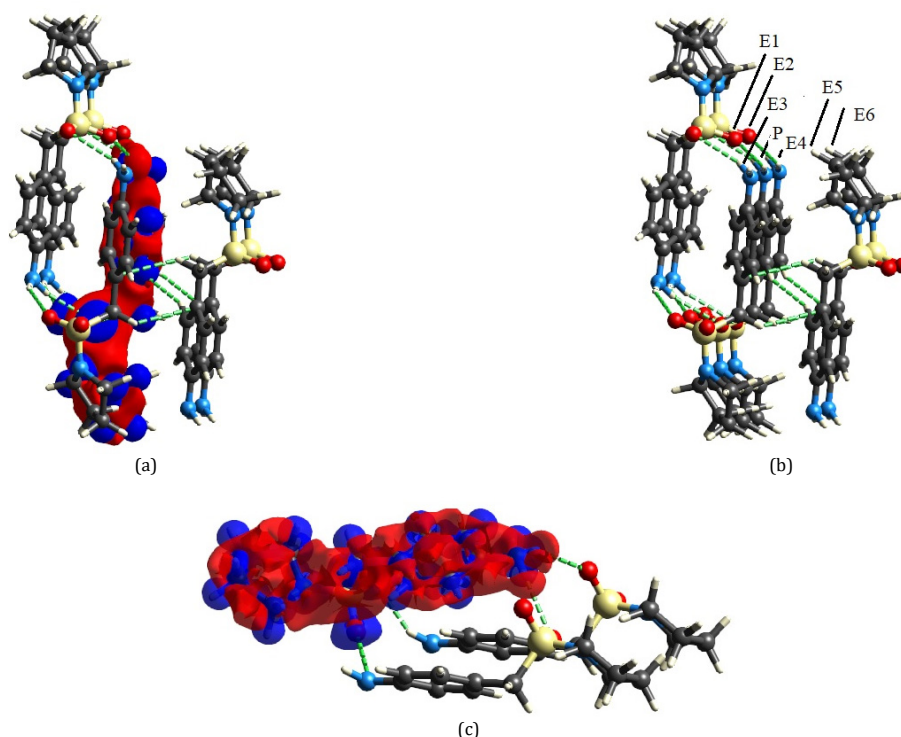
Figure 9. Electrostatic deformation density maps (a) Promolecule's electron density interaction with nearby molecules, (b) Promolecules (P) interaction with the surrounding molecules (E₁-E₆), and (c) Specific interaction of surrounding molecules with the promolecule's electron density.

3.3.4. Fingerprint plots

The complex three-dimensional intermolecular interactions in molecular crystal simplified in two-dimensional visual presentation of the frequency of each combination of d_e and d_i across the surface of a molecule including the extent of interaction of a particular type through the relative area obtained from HFS is specifically known as 'Fingerprint Plot' [45]. Quantification and segregation of intermolecular interactions/contacts between inside and outside the HFS has been achieved through the 2D plot generated in terms of d_e, d_i pairs in intervals of 0.01. The total interactions in the crystal packing involving all types of interactions, especially H⋯H, O⋯H, and N⋯H contacts comprising 100% appears in Figure 10a with wings type areas, symmetrically placed on either side of the spike at the middle of the 2D plot. The interactions/contacts representing H⋯H, O-H/H-O, C-H/H-C/C-H and N-H/H-N as shown in Figure 10b, c, d and e include the remaining as grey area. The short-distance H⋯H interaction has the maximum contribution of 53.7% and occurs along the diagonal. The intensity of this is maximum around $d_e = d_i \sim 1.05$ Å, ($d_e + d_i \sim 2.1$ Å) Figure 10b with a display of blue colored sharp spike, probably largely due to aromatic protons followed by methylene and five membered ring protons. The other interactions along with their reciprocals are segregated and displayed in Figures 10c, d, and e. The overall O⋯H/H⋯O interaction that contributes to the extent of 24.3% at $d_e = d_i \sim 1.35$ Å ($d_e + d_i \sim 2.7$ Å) follows the H⋯H interaction. The next dominating contacts of 16.4% and 5.1% are due to C⋯H/H⋯C ($d_e = d_i \sim 1.65$ Å; d_e +di

~ 3.3 Å) and N⋯H / H…N ($d_e = d_i \sim 1.55$ Å; $d_e + d_i \sim 3,1$ Å), respectively. Except C⋯C of negligibly small quantity of 0.3%, no other contacts are observed. The various possible combinations of atom-pair interactions and the individual contributions to the overall interaction are shown in the interaction-matrix Table 4. It is clearly evident that short interatomic H…H interactions (53.7%) with intense scattering is the major contributor to the crystal packing. Interestingly the symmetric or slightly asymmetric distribution of bins of X⋯Y/Y⋯X interactions, over the HSF can be found by inspecting the off-diagonal elements in green color (X⋯X) in the Table 4 shown as couple of spikes with the tips at $d_e + d_i \sim 2.7$ Å. Thus, for the packing pattern of the crystal structure, the major contribution is from H⋯H followed by O⋯H/H⋯O, C⋯/H⋯C and N⋯H/H⋯N interactions and these contacts have been meticulously taken into account to construct the three-dimensional crystal packing arrangement shown in Figure 11.

3.3.5. Interaction energies and energy framework

In crystal engineering, an understanding of intermolecular interaction energies is essential for the design of new crystalline solids with desired physicochemical properties [46-48]. In the crystalline state containing the three-dimensional regular patterns of molecules, each molecule is systematically surrounded by nearby molecules, giving rise to resultant stabilizing interactions between a pair of molecules along with minimized repulsive interactions, and such interactions may be considered to act between the centroids (based only on the
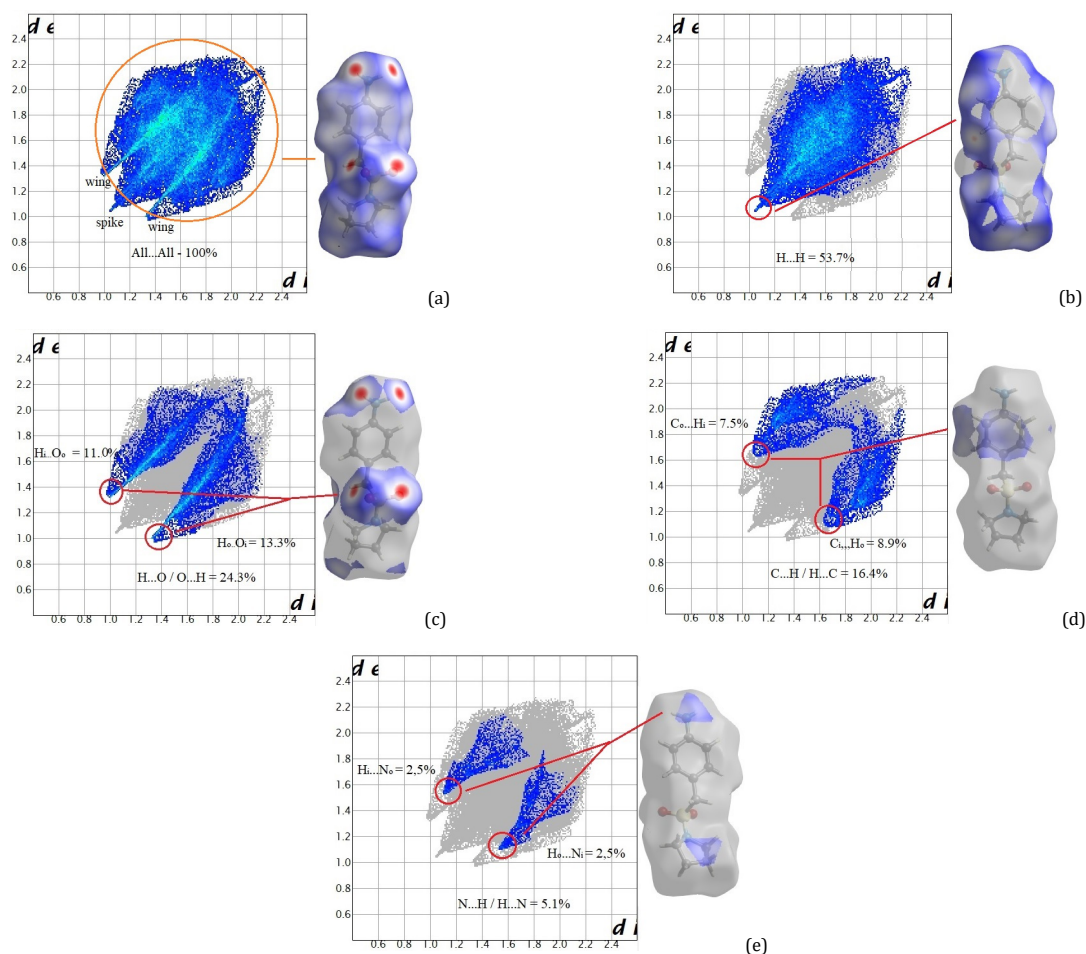
Figure 10. Two-dimensional finger print plots of PSMA (a) all contacts, (b) H-H, (c) H-O/O-H, (d) C-H/H-C, and (e) N-H/H-N.
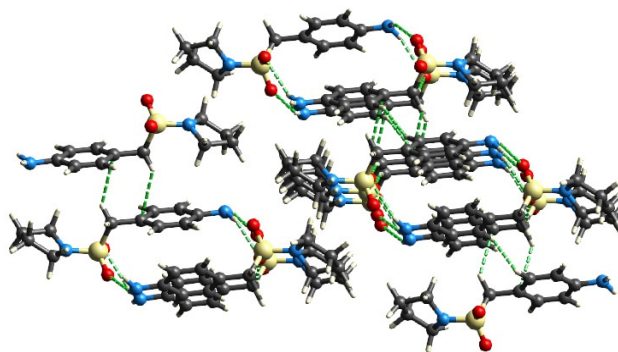
Figure 11. The three-dimensional crystal packing arrangement.

coordinates of all atoms and not centres of mass) of the participating molecules. The total interaction energy is generally expressed in terms of four key components: electrostatic, polarization, dispersion, and exchange-repulsion:

$$E_{tot} = k_{ele}E_{ele} + k_{pol}E_{pol} + k_{dis}E_{dis} + k_{rep}E_{rep} \qquad (2)$$

The E_{tot} is evaluated through CE-B3LYP/6-31G(d,p) implemented in CrystalExplorer 17.5, by computing the individual components using the monomer wave functions that have been appropriately scaled (k_{ele} = 1.057, k_{pol} = 0.740, k_{dis} = 0.871 and k_{rep} = 0.618) to reproduce the counterpoise-corrected energies B3LYP-D2/6-31G(d,p) with a small mean absolute deviation of 2.4 kJ/ mol [33,46]. For this, the reference PSMA molecule from

the CIF file was first created followed by the creation and fragment completion of a cluster holding 13 PSMA molecules around it within 3.8 Å. The holistic picture of the cluster reveals the linear disposition of the PSMA molecules shown in Figure 12. After the appropriate keywords have been selected, the interaction energies between the centroids of molecular pairs having the reference at the centre within the cluster have been computed with the computed wave functions.

The various interaction energies (E_{tot}) of the reference molecule with the specific nearby molecule(s) with breakup details (unscaled) into electrostatic, polarization, dispersion and exchange repulsion, (E_{ele}, E_{pol}, E_{dis} and E_{rep}) seem to be the critical controlling factors in crystal packing and are shown in the following Table 5.

Table 5. The interaction energies (kJ/mol) of the reference (R) with the surrounding molecules (E1 to E13) within 3.8 Å from PSMA R is the distance between the molecular centroids (mean atomic position) in Å.

Color	N	Symmetry operation	R	E_{ele}	E_{po}	E_{dis}	E_{rep}	E_{tot}
(red)	1	-x, -y, -z	12.35	0.5	-0.5	-11.8	7.7	-5.4
(orange)	2	x+1/2, -y+1/2, z+1/2	8.44	-6.1	-1.2	-2.9	0.1	-9.8
(yellow-green)	2	x, y, z	13.74	1.2	-0.4	-5.0	1.5	-2.4
(green)	1	-x, -y, -z	6.33	3.0	-1.3	-22.7	13.2	-9.4
(cyan)	2	x, y, z	5.81	-5.4	-5.4	-28.0	18.0	-22.9
(blue)	2	-x+1/2, y+1/2, -z+1/2	7.45	-32.8	-9.8	-34.1	30.5	-52.8
(purple)	2	-x+1/2, y+1/2, -z+1/2	8.80	-13.0	-4.2	-20.3	11.6	-27.4
(magenta)	1	-x, -y, -z	5.09	-19.8	-5.5	-55.6	34.6	-52.1

*B3LYP/6-31G(d, p) electron density is used N - number of pairs with that energy, Symop - relates that particular color coded molecule with the central molecule. Scale factors for B3LYP/6-31G(d,p): 1.057 (k_{ele}), 0.740 (k_{pol}), 0.871 (k_{dis}) and 0.618 (k_{rep}).

Table 6. Computed λ_{max} (λ_{cal}), excitation energy (E) and oscillator strengths of PSMA.

Excitation no	$\lambda_{Cal.}$ (nm)	E (eV)	*f*osc. strength	Assignment
1	271.22	4.5710	0.0300	π-π*
2	251.36	4.9324	0.4765	π-π*
4	237.76	5.2147	0.0203	π-π*
13	204.26	6.0698	0.1836	π-π*
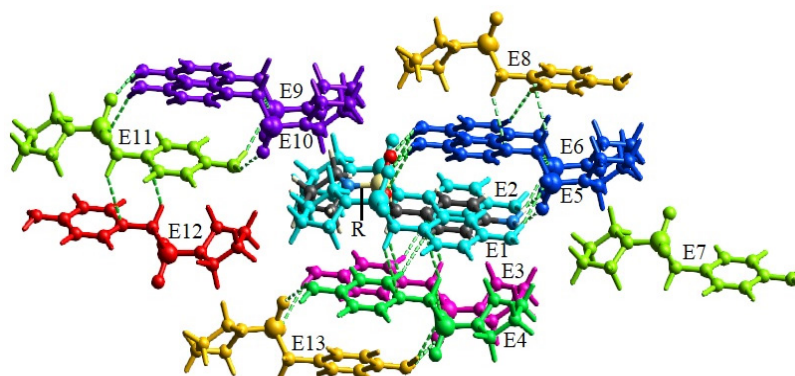
Figure 12. Intermolecular interactions with various color codes.

The color code in the first column represents color of the surrounding molecules (Figure 12), labelled from E1 to E13 around R. The last column of the table provides the sum of the scaled values of the individual components (unscaled). Analyzing the energy components of 13 pairs comprising R and E1 to E13, the contribution of E_{dis} to E_{tot} is overwhelming, resulting in crystal stabilization, except in two pairs at a distance of 8.44 Å in which E_{ele} is twice the E_{pol}. The higher dispersion energy -55.6 kJ/mol of the R-E3 pair whose centroids are 5.09 Å apart has intermolecular hydrogen bond interaction through >SO₂ and -NH₂ units reciprocally, followed by the R-E5 and R -E6 pairs with centroids 7.45 Å apart (-17.05 kJ/mol). Thus, the strength of the hydrogen bond interaction may be roughly quantified in terms of E_{dis} provided if R is relatively low.

Energy framework is a picturesque representation of intermolecular interactions that would help to have a clear idea about crystal packing. The reference molecule PSMA generated from the CIF file is used to simulate a group of 1×1×1 unit cells, which encompasses 12 molecules after the completion of all molecular fragments. For this cluster total as well as the corresponding energy components have been estimated at CE-B3LYP/6-31G(d,p) to construct the energy frameworks of coulomb energy, dispersion energy and total energy [47] in the form of scaled cylinders of 100. Total energy components less than 10 kJ/mole have been dropped for clarity, as shown in Figure 13a-d. The relative strengths of vectorial interaction energies are correlated with the size of the cylinders. Comparison of the dimensions of cylinders in the energy frameworks substantiate that the dispersion energy contribution to the total energy is significant to the crystal packing, and this is followed by electrostatic interaction of the charge distribution among the interacting monomers. Figure 13d shows that the |E_{tot}| is inversely related to the distance between the centroids of the interacting pair.

3.4. Electronic spectral analysis of PSMA

The electronic excitation in the UV-Visible region of PSMA in methanol medium measured experimentally is shown in Figure 14 and the prominent transition wavelength (λ_{max}) has been observed at 251 nm.

The adiabatic excitation energies have been computed with TD-DFT in methanol solvent for the optimized geometry using 6-311++G(d,p) basis set for 40 excited states. The results reveal that the most probable electronic transitions are those with oscillator strengths (*f*) 0.03, 0.4765, 0.0203, 0.1836, and 0.6868 corresponding to the excitation states 1, 2, 4, 13 and 19, respectively. The theoretically simulated electronic spectrum is shown in Figure 15. The first transition occurs from HOMO to LUMO (MO-64→MO-65). All singlet excitations with appreciable oscillator strengths have been collected in Table 6.

Figure 13. Energy framework diagram for (a) coulomb energy component, (b) dispersion energy component, (c) total energy, and (d) total energy annotated.

No.	P/V	Wavelength	Abs.
1	⊕	355.80	0.002
2	⊕	251.20	0.019
3	⊕	215.20	0.577

Figure 14. Experimental UV-visible spectrum of PSMA.

Figure 15. Theoretical UV - visible spectrum of PSMA.

The experimentally observed absorption at 251 nm exactly coincides with the calculated second excitation (251.35 nm) involving electron transfer from HOMO-2 (MO-62) and HOMO (MO-64) to LUMO (MO-65), LUMO+1 (MO-66) and LUMO+2 (MO-67). To eliminate the multiple excitations and to identify the dominant component, the corresponding NTOs have generated to recognize the NTO transition from excited particle (occupied) to the empty hole (unoccupied) [49] showing the chemical intuition of excitation. The direct TD-DFT calculation has provided three combinations on a canonical basis, whereas NTO has given a better conceptualization of HOMO to LUMO excitation to the extent of 95.5% as shown in Figure 16 at 251.36 nm, 4.9324 eV being the excitation energy. The absorptions calculated around 200 nm with higher probability values indicated by *f* values of 0.6868 and 0.1836 fall in the vacuum UV region are absent in the experimentally recorded spectrum.

Figure 16. HOMO-LUMO transition based on NTOs.
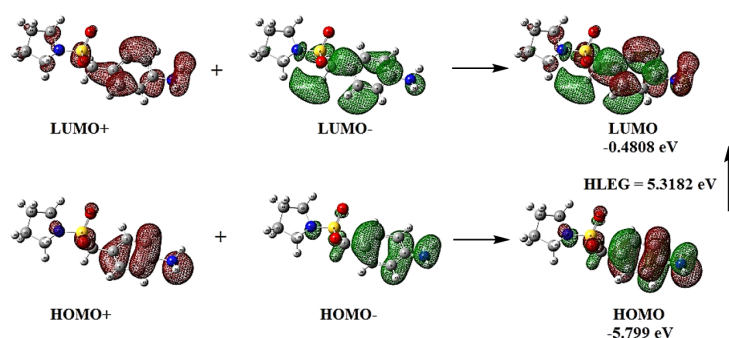
Figure 17. HOMO-LUMO structures of PSMA.

3.5. Frontier molecular orbital studies

Among the molecular orbitals, HOMO is the one with the highest eigen value and has a pair/single electron occupied in it and the next virtual orbital is the LUMO. Due to their position, they are called Frontier Molecular Orbitals (FMOs) and play an important role in the chemical stability, reactivity, charge transfer process, photoexcitation, magnetism, and molecular electronics of the molecule [50]. Kohn Sham (KS) orbitals of density functional theory give a theoretical and practical basis for a better qualitative understanding of molecular orbitals [51-53] even though the DFT functional may not evaluate orbital eigenvalues precisely. If the HOMO-LUMO energy gap, namely HLEG is small, it indicates that there is more intramolecular charge transfer from the electron-releasing to the electron-accepting groups through π-conjugation [54]. The fact that chemical stability is directly proportional to the HLEG value [55, 56] has been used to analyze bioactivity in terms of intra-molecular charge transfer [57-59].

The positive and negative parts of the 64 (HOMO) and 65 (LUMO) eigenvectors and the respective graphical represent-tations of the combined functions with an isovalue of 0.02 are shown in Figure 17. Inspection of HOMO and LUMO surfaces indicates that AOs from the heavy atoms of benzene skeleton contribute in the construct of π-type HOMO and π*-LUMO. As the energy gap (HLEG of 5.3182 eV) between these two FMOs is of considerable magnitude, PSMA seems to be a thermodynamically stable species with a subdued chemical activity [59].

The chemical reaction of a substrate PSMA with an electro-phile or a nucleophile is largely controlled by the HMO-LUMO energies of the participating species in addition to their symmetry, i.e., an electrophilic reaction is favored if the reagent's LUMO lies nearer to the high HOMO of the substrate while latter's LUMO proximity to the reagent's HOMO enhances nucleophilic reaction, provided thermodynamic stability of the substrate is not favored [59].

4. Conclusions

4-((Pyrrolidin-1-ylsulfonyl) methyl) aniline (PSMA) was crystalized and its structural features were analyzed including the various strong and weak intermolecular interactions resulting in its supramolecular architecture. DFT calculations were performed to compare the experimental and theoretically calculated geometrical parameters of the molecule and the results indicate a good correlation. Hirshfeld surface analysis was carried out and it was observed that among the various intermolecular interactions, the H···H dispersive interactions play a major role apart from the other interactions for the crystal packing and the energy frame work had been studied. The observed UV-visible spectrum was found to be in fairly good/satisfactory agreement with the one theoretically simulated by HOMO-LUMO calculations. The results obtained may stimulate further interest on PSMA and related compounds for future experimental and theoretical investigations.

Acknowledgements

Supporting information Ⓢ

CCDC-2100572 contains the supplementary crystallographic data for this paper. These data can be obtained free of charge via www.ccdc.cam.ac.uk/data_request/cif, or by e-mailing data_request@ccdc.cam.ac.uk, or by contacting The Cambridge Crystallographic Data Centre, 12 Union Road, Cambridge CB2 1EZ, UK; fax: +44(0)1223-336033.

Disclosure statement ⅮⅭ

Conflict of interest: The authors declare that they have no conflict of interest.
Ethical approval: All ethical guidelines have been adhered.
Sample availability: Samples of the compounds are available from the author.

CRediT authorship contribution statement ℂℝ

Conceptualization: Sethuraman Velusamy, Soundararajan Krishnan; Methodology: Sethuraman Velusamy, Ramalingam Marimuthu; Software: Thanigaimani Kaliyaperumal, Ramalingam Marimuthu; Validation: Thanigaimani Kaliyaperumal, Ramalingam Marimuthu; Formal Analysis: Soundararajan Krishnan, Sethuraman Velusamy; Investigation: Soundararajan Krishnan; Data Curation: Soundararajan Krishnan; Writing - Original Draft: Soundararajan Krishnan, Sethuraman Velusamy; Writing - Review and Editing: Sethuraman Velusamy, Ramalingam Marimuthu; Visualization: Soundararajan Krishnan, Ramalingam Marimuthu; Funding acquisition: No funding from any funding bodies; Supervision: Sethuraman Velusamy, Ramalingam Marimuthu; Project Administration: Soundararajan Krishnan, Thanigaimani Kaliyaperumal, Ramalingam Marimuthu, Sethuraman Velusamy.

ORCID ⅮⅮ

Soundararajan Krishnan
 https://orcid.org/0000-0003-4167-6931
Thanigaimani Kaliyaperumal
 https://orcid.org/0000-0002-4384-7848
Ramalingam Marimuthu
 https://orcid.org/0000-0002-0551-5164
Sethuraman Velusamy
 https://orcid.org/0000-0003-4449-3858

References

[1].   Wilcox, R. W. *Medical News* **1900**, *15*, 931–932.
[2].   Bentley, R. *J. Ind. Microbiol. Biotechnol.* **2009**, *36* (6), 775–786.
[3].   Sonu; Rabiya Parveen, B.; Praveen, S.; Pal, H. *Int. J. Pharm. Chem.* **2017**, *7* (5), 70–73.
[4].   Iqbal, R.; Zareef, M.; Ahmed, S.; Zaidi, J. H.; Arfan, M.; Shafique, M.; Al-Masoudi, N. A. *J. Chin. Chem. Soc.* **2006**, *53* (3), 689–696.
[5].   Saingar, S.; Kumar, R.; Joshi, Y. C. *Med. Chem. Res.* **2011**, *20* (7), 975–980.
[6].   Schreiber, K. J.; Austin, R. S.; Gong, Y.; Zhang, J.; Fung, P.; Wang, P. W.; Guttman, D. S.; Desveaux, D. *BMC Plant Biol.* **2012**, *12* (1), 226–235.
[7].   Shah, S. S. A.; Rivera, G.; Ashfaq, M. *Mini Rev. Med. Chem.* **2013**, *13* (1), 70–86.
[8].   Supuran, C. T. *Curr. Med. Chem.* **2012**, *19* (6), 831–844.
[9].   Wulf, N. R.; Matuszewski, K. A. *Am. J. Health. Syst. Pharm.* **2013**, *70* (17), 1483–1494.
[10]. Owa, T.; Nagasu, T. *Expert Opin. Ther. Pat.* **2000**, *10* (11), 1725–1740.
[11]. Supuran, C. T.; Scozzafava, A.; Casini, A. *Med. Res. Rev.* **2003**, *23* (2), 146–189.
[12]. Supuran, C. T.; Scozzafava, A. *Expert Opin. Ther. Pat.* **2002**, *12* (2), 217–242.
[13]. Supuran, C.; Scozzafava, A. *Curr. Med. Chem. Immunol. Endocr. Metab. Agents* **2001**, *1* (1), 61–97.
[14]. Maren, T. H. *Annu. Rev. Pharmacol. Toxicol.* **1976**, *16* (1), 309–327.
[15]. Supuran, C. T.; Conroy, C. W.; Maren, T. H. *Eur. J. Med. Chem.* **1996**, *31* (11), 843–846.
[16]. Boyd, A. E. *Diabetes* **1988**, *37* (7), 847–850.
[17]. Thaisrivongs, S.; Skulnick, H. I.; Turner, S. R.; Strohbach, J. W.; Tommasi, R. A.; Johnson, P. D.; Aristoff, P. A.; Judge, T. M.; Gammill, R. B.; Morris, J. K.; Romines, K. R.; Chrusciel, R. A.; Hinshaw, R. R.; Chong, K. T.; Tarpley, W. G.; Poppe, S. M.; Slade, D. E.; Lynn, J. C.; Horng, M. M.; Tomich, P. K.; Seest, E. P.; Dolak, L. A.; Howe, W. J.; Howard, G. M.; Watenpaugh, K. D. *J. Med. Chem.* **1996**, *39* (22), 4349–4353.
[18]. Supuran, C. T.; Scozzafava, A.; Clare, B. W. *Med. Res. Rev.* **2002**, *22* (4), 329–372.
[19]. Scozzafava, A.; Supuran, C. T. *J. Med. Chem.* **2000**, *43* (20), 3677–3687.
[20]. Thornber, C. W. *Chem. Soc. Rev.* **1979**, *8* (4), 563–580.
[21]. Lavanya, R. *Inter. J. Pharm. Sci. Invent.* **2017**, *6* (2), 1-3.
[22]. Keam, S. J.; Goa, K. L.; Figgitt, D. P. *Drugs* **2002**, *62* (2), 387–414.
[23]. Manikandan, D.; Swaminathan, J.; Tagore, S. S.; Gomathi, S.; Sabarinathan, N.; Ramalingam, M.; Balasubramani, K.; Sethuraman, V. *Spectrochim. Acta A Mol. Biomol. Spectrosc.* **2020**, *239* (118484), 118484.
[24]. Bruker, SMART APEX2, SAINT ABD SADABS, Bruker AXS Inc., Madison, Wisconsin, USA, 2008.
[25]. Sheldrick, G. M *Acta Crystallogr. A* **2008**, *64* (Pt 1), 112–122.
[26]. Sheldrick, G. M. *Acta Crystallogr. A Found. Adv.* **2015**, *71* (Pt 1), 3–8.
[27]. Becke, A. D. *J. Chem. Phys.* **1993**, *98* (7), 5648–5652.
[28]. Frisch, M. J.; Trucks G. W.; Schlegel, H. B.; Scuseria, G. E.; Robb, M. A.; Cheeseman, J. R.; Scalmani, G.; Barone, V.; Mennucci, B.; Petersson, G. A.; Nakatsuji, H.; Caricato, M.; Li, X.; Hratchian, H. P.; Izmaylov, A. F.; Bloino, J.; Zheng, G.; Sonnenberg, J. L.; Hada, M.; Ehara, M.; Toyota, K.; Fukuda, R.; Hasegawa, J.; Ishida, M.; Nakajima, T.; Honda, Y.; Kitao, O.; Nakai, H.; Vreven, T.; Montgomery, J. A.; Peralta, J. E.; Ogliaro, F.; Bearpark, M.; Heyd, J. J.; Brothers, E.; Kudin, K. N.; Staroverov, V. N.; Kobayashi, R.; Normand, J.; Raghavachari, K.; Rendell, A.; Burant, J. C.; Iyengar, S. S.; Tomasi, J.; Cossi, M.; Rega, N.; Millam, J. M.; Klene, M.; Knox, J. E.; Cross, J. B.; Bakken, V.; Adamo, C.; Jaramillo, J.; Gomperts, R.; Stratmann, R. E.; Yazyev, O.; A. J. Austin, A. J.; Cammi, R.; Pomelli, C.; Ochterski, J. W.; Martin, R. L.; Morokuma, K.; Zakrzewski, V. G; Voth, G. A.; Salvador, P.; Dannenberg, J. J.; Dapprich, S.; Daniels, A. D.; Farkas, O.; Foresman, J. B.; Ortiz, J. V.; Cioslowski, J.; Fox, D. J. Gaussian, Inc. , Gaussian 03, Revision E.01, Wallingford CT, 2004.
[29]. Frisch, M. J.; Trucks G. W.; Schlegel, H. B.; Scuseria, G. E.; Robb, M. A.; Cheeseman, J. R.; Scalmani, G.; Barone, V.; Mennucci, B.; Petersson, G. A.; Nakatsuji, H.; Caricato, M.; Li, X.; Hratchian, H. P.; Izmaylov, A. F.; Bloino, J.; Zheng, G.; Sonnenberg, J. L.; Hada, M.; Ehara, M.; Toyota, K.; Fukuda, R.; Hasegawa, J.; Ishida, M.; Nakajima, T.; Honda, Y.; Kitao, O.; Nakai, H.; Vreven, T.; Montgomery, J. A.; Peralta, J. E.; Ogliaro, F.; Bearpark, M.; Heyd, J. J.; Brothers, E.; Kudin, K. N.; Staroverov, V. N.; Kobayashi, R.; Normand, J.; Raghavachari, K.; Rendell, A.; Burant, J. C.; Iyengar, S. S.; Tomasi, J.; Cossi, M.; Rega, N.; Millam, J. M.; Klene, M.; Knox, J. E.; Cross, J. B.; Bakken, V.; Adamo, C.; Jaramillo, J.; Gomperts, R.; Stratmann, R. E.; Yazyev, O.; A. J. Austin, A. J.; Cammi, R.; Pomelli, C.; Ochterski, J. W.; Martin, R. L.; Morokuma, K.; Zakrzewski, V. G; Voth, G. A.; Salvador, P.; Dannenberg, J. J.; Dapprich, S.; Daniels, A. D.; Farkas, O.; Foresman, J. B.; Ortiz, J. V.; Cioslowski, J.; Fox, D. J. Gaussian, Inc. , Gaussian 09, Revision B.01, Wallingford CT, 2010.
[30]. Ortmann, F.; Bechstedt, F.; Schmidt, W. G. *Phys. Rev. B* **2006**, *73* (20), 205101, 1–10.
[31]. Hirshfeld, F. L. *Theoret. Chim. Acta* **1977**, *44* (2), 129–138.
[32]. Spackman, M. A.; Byrom, P. G. *Chem. Phys. Lett.* **1997**, *267* (3–4), 215–220.
[33]. Mackenzie, C. F.; Spackman, P. R.; Jayatilaka, D.; Spackman, M. A. *IUCrJ* **2017**, *4* (Pt 5), 575–587.
[34]. Malenov, D. P.; Janjić, G. V.; Medaković, V. B.; Hall, M. B.; Zarić, S. D. *Coord. Chem. Rev.* **2017**, *345*, 318–341.
[35]. McKinnon, J. J.; Jayatilaka, D.; Spackman, M. A. *Chem. Commun. (Camb.)* **2007**, No. 37, 3814–3816.
[36]. Allen, F. H.; Kennard, O.; Watson, D. G.; Brammer, L.; Guy Orpen, A.; Taylor, R. *J. Chem. Soc. Perkin Trans. 2* **1987**, 12, S1–S19.
[37]. Ravikumar, K.; Sridhar, B.; Krishnan, H.; Singh, A. N. *Acta Crystallogr. C* **2008**, *64* (Pt 1), o15-7.
[38]. Sridhar, B.; Ravikumar, K.; Krishnan, H.; Singh, A. N. *J. Chem. Crystallogr.* **2011**, *41* (3), 291–296.
[39]. Spackman, M. A.; Jayatilaka, D. *CrystEngComm* **2009**, *11* (1), 19–32.
[40]. Koenderink, J. J.; van Doorn, A. J. *Image Vis. Comput.* **1992**, *10* (8), 557–564.
[41]. Koenderink, J. J. *Solid Shape*; MIT Press: London, England, 1990.
[42]. Bondi, A. *J. Phys. Chem.* **1964**, *68* (3), 441–451.
[43]. Gumus, I.; Solmaz, U.; Gonca, S.; Arslan, H. *Eur. J. Chem.* **2017**, *8* (4), 349–357.
[44]. Khan, I.; Panini, P.; Khan, S. U.-D.; Rana, U. A.; Andleeb, H.; Chopra, D.; Hameed, S.; Simpson, J. *Cryst. Growth Des.* **2016**, *16* (3), 1371–1386.
[45]. Spackman, M. A.; McKinnon, J J *CrystEngComm* **2002**, *4* (66), 378–392.
[46]. Turner, M. J.; Grabowsky, S.; Jayatilaka, D.; Spackman, M. A. *J. Phys. Chem. Lett.* **2014**, *5* (24), 4249–4255.
[47]. Spackman, M. A.; Spackman, P. R.; Thomas, S. P. 13 Beyond Hirshfeld Surface Analysis: Interaction Energies, Energy Frameworks and Lattice Energies with CrystalExplorer. In *Complementary Bonding Analysis*; De Gruyter, 2021; pp 329–352.

[48]. Maginn, S. J. *J. Appl. Crystallogr.* **1991**, *24* (3), 265–265.

[49]. Martin, R. L. *J. Chem. Phys.* **2003**, *118* (11), 4775–4777.

[50]. Stowasser, R.; Hoffmann, R. *J. Am. Chem. Soc.* **1999**, *121* (14), 3414–3420.

[51]. Zhang, G.; Musgrave, C. B. *J. Phys. Chem. A* **2007**, *111* (8), 1554–1561.

[52]. Zhan, C.-G.; Nichols, J. A.; Dixon, D. A. *J. Phys. Chem. A* **2003**, *107* (20), 4184–4195.

[53]. Gunasekaran, S.; Arun Balaji, R.; Kumaresan, S.; Anand, G.; Srinivasan, S. *Can. J. Anal. Sci. Spectrosc.* **2008**, *53*, 149-162.

[54]. Lewis, D. F. V.; Ioannides, C.; Parke, D. V. *Xenobiotica* **1994**, *24* (5), 401–408.

[55]. Padmaja, L.; Ravikumar, C.; Sajan, D.; Hubert Joe, I.; Jayakumar, V. S.; Pettit, G. R.; Faurskov Nielsen, O. *J. Raman Spectrosc.* **2009**, *40* (4), 419–428.

[56]. Ravikumar, C.; Joe, I. H.; Jayakumar, V. S. *Chem. Phys. Lett.* **2008**, *460* (4–6), 552–558.

[57]. Pîrnău, A.; Chiş, V.; Oniga, O.; Leopold, N.; Szabo, L.; Baias, M.; Cozar, O. *Vib. Spectrosc.* **2008**, *48* (2), 289–296.

[58]. Liu, S. *J. Chem. Sci. (Bangalore)* **2005**, *117* (5), 477–483.

[59]. Sharmila Tagore, S.; Swaminathan, J.; Manikandan, D.; Gomathi, S.; Sabarinathan, N.; Ramalingam, M.; Sethuraman, V. *Heliyon* **2021**, *7* (4), e06593.